Search for entrance channel effects in sub-barrier fusion reactions

A. Charlop, J. Bierman, Z. Drebi, A. Garcia,* S. Gil,† D. Prindle, A. Sonzogni, R. Vandenbosch, and D. Ye
University of Washington, Nuclear Physics Laboratory GL-10, Seattle, Washington 98195
(Received 2 May 1994)

In order to explore the possibility that previously observed anomalous mean angular momenta are related to the mass asymmetry of the entrance channel, we have studied three systems, ^{28}Si + ^{142}Ce, ^{32}S + ^{138}Ba, and ^{48}Ti + ^{122}Sn, all of which lead to the same compound nucleus, ^{170}Hf. Gamma ray multiplicities for fusion have been determined using an electrostatic deflector and time of flight to identify the evaporation residues. Results have been obtained for bombarding energies from approximately 20% above the Coulomb barrier down to nearly 10% below the barrier. The mean angular momenta deduced from the gamma ray multiplicities are generally well reproduced by coupled channels calculations employing known deformation parameters and an estimate of the transfer strength and do not show any evidence of an unexpected effect related to the mass asymmetry of the entrance channel.

PACS number(s): 25.70.Jj

I. INTRODUCTION

The study of heavy-ion fusion has been a major topic of interest for many years. It is well established that the fusion cross section is greatly enhanced in the energy region near and below the Coulomb barrier when compared to simple one-dimensional barrier penetration models that reproduce the fusion excitation function at higher energies [1–3].

The enhancement of the fusion cross section has been attributed to a number of different mechanisms. One class of models incorporates additional degrees of freedom that can lead to fusion such as exciting low-lying collective states [4,5] in the projectile or target nucleus or nucleon transfer [6,7] before fusion. Another approach is to introduce a neck degree of freedom [8,9]. Yet another approach is to invoke absorption under the barrier [10,11]. Recently the interacting boson model has been used to study sub-barrier fusion reactions [12].

Usual measurements of the fusion excitation function alone do not contain sufficient information to give a stringent test of fusion models. High-precision measurements of the fusion excitation function [13–15] or measurement of one or more of the higher moments of the partial wave distribution are necessary to provide a good test of fusion models. The simplest moment to determine experimentally is the first moment of the partial-wave distribution, the mean spin $\langle l \rangle$. This can be determined experimentally from γ-ray multiplicities [16–18], isomer ratios [19], and rotational state distributions [20]. A closely related quantity, the rms spin $\langle l^2 \rangle^{1/2}$, can be determined from fission fragment angular distributions [21].

Generally, fusion models are able to reproduce the fusion excitation function quite reasonably. However, even when the models give a reasonable fit to the fusion excitation function, they often fail to reproduce the $\langle l \rangle$ of the compound nucleus in the region of the fusion barrier. A recent review article [3] on angular momentum distributions in sub-barrier fusion, summarized the available data by showing the systematics of $\langle l \rangle_{\text{expt}}/\langle l \rangle_{\text{theor}}$ as a function of the center-of-mass energy relative to the fusion barrier for the systems where both the fusion cross sections and $\langle l \rangle$ have been measured. Although for all of the systems shown the fusion excitation functions were well reproduced by the fusion model that calculated $\langle l \rangle_{\text{theor}}$, the experimental $\langle l \rangle$'s were greater than the model predictions by up to factors of 2 in some cases. The deviations are largest at energies below the barrier. There are also some indications that the discrepancy is greater for heavy symmetric systems than for light asymmetric systems. This suggests that fusion below the barrier may be affected by the mass asymmetry of the entrance channel. Such an effect has been observed in a comparison of the ^{32}S + ^{100}Mo and ^{36}S + ^{96}Mo systems [22].

In order to investigate the possibility of an entrance channel effect, it was decided to measure the fusion excitation functions and γ multiplicities for a series of target and projectile systems that lead to the same compound nucleus. The compound nucleus ^{170}Hf was chosen for this study. This compound nucleus is in the same mass region as the systems that show the largest discrepancies with the models [17,18,23,24]. Three projectile and target combinations were used, ^{28}Si + ^{142}Ce, ^{32}S + ^{138}Ba, and ^{48}Ti + ^{122}Sn. The reduced masses in these systems are 23.4, 26.0, and 34.4, respectively, giving nearly a 50% increase in the reduced mass for this study. The possible role of the reduced mass (a measure of entrance channel mass asymmetry for systems leading to the same compound nucleus) is discussed in [25].

In this paper, we report the γ multiplicity measurements for the three systems in this study. The evapora-

*Present address: University of Notre Dame, Notre Dame, IN 46556.
†Present address: Tandar, Departmento de Fisica, CNEA, Buenos Aires, Argentina.

tion residue cross sections and fusion-fission cross sections for all three systems were measured in separate experiments and are presented elsewhere [25,26]. An overview of these results have been presented in a recent Rapid Communication [27]. In the next section we present the experimental setup and results for the γ-multiplicity measurements. In the following sections we discuss the conversion of the γ-multiplicity information to mean spin. We then discuss the analysis of these results along with those from [25,26] to look for evidence of a mass asymmetry effect in sub-barrier fusion.

II. EXPERIMENTAL SETUP AND RESULTS

The γ multiplicities for three systems were measured using the electrostatic deflector at the University of Washington Nuclear Physics Laboratory. Beams of ^{28}Si, ^{32}S, and ^{48}Ti were produced using the 9 MV tandem accelerator and superconducting booster accelerator (Linac) at the Nuclear Physics Laboratory. The ^{142}Ce, ^{138}Ba, and ^{122}Sn targets had a thickness (isotopic purity) of 160 $\pm$ 10 μg/cm^2 (> 90%), 172 $\pm$ 10 μg/cm^2 (99.67%), and 200 $\pm$ 10 μg/cm^2 (92.20%), respectively [28]. All of the targets were produced by evaporation on to 30 μg/cm^2 ^{12}C foils.

The beam energies covered a range of energies from approximately 20% above the Coulomb barrier down to nearly 10% below the barrier. Table I lists the energies and γ multiplicities measured for each system. The fusion cross sections in this energy region range from about 1 mb to several hundred mb [25].

An electrostatic deflector was used to separate the evaporation residues (ER's) from the projectile-like fragments. The ER's were then detected using a 100 μm silicon strip detector that was offset from the beam axis. The detector consisted of seven strips each about 0.9 cm wide by 4 cm high and were separated by a 100 μm gap. For the γ-multiplicity measurements the detector was used in a reversed bias mode which effectively creates a detector that is 6.3 cm wide by 4 cm high with no position sensitivity. The ER's were identified by measuring the time of flight (TOF) relative to the timing structure of the Linac booster. The beam was chopped to produce a gap of 240 nsec between beam bursts.

The ER's were detected both in singles mode and in coincidence with γ rays in any one of three 7.6 cm $\times$7.6 cm NaI(Tl) γ detectors placed around the target. Two of the NaI(Tl) detectors were placed at $\pm$140° and the third was placed at +65° with respect to the beam direction. In front of each of the detectors was placed an absorber made of 1.8 mm of Pb and 1.0 mm of Cu. The Pb absorber stopped γ rays of less than 100 keV from entering the detector. The Cu absorber was between the detector and the Pb to stop the x rays produced in the Pb absorber from entering the detectors. The absolute efficiencies of the NaI(Tl) detectors were measured using calibrated ^{57}Co, ^{60}Co, ^{137}Cs, and ^{88}Y sources that were placed in the target position. The efficiency of the detectors was essentially flat between 200 keV and 1.8 MeV. The combined efficiency of the three NaI detectors was approximately 2% for γ rays above 200 keV in energy.

TABLE I. Experimental γ multiplicities (M_γ) for ^{28}Si + ^{142}Ce, ^{32}S + ^{138}Ba, and ^{48}Ti + ^{122}Sn. Column 3 (dM_γ) lists the statistical error for each measurement.

^{28}Si + ^{142}Ce			^{32}S + ^{138}Ba			^{48}Ti + ^{122}Sn		
E_{lab} (MeV)	M_γ	dM_γ	E_{lab} (MeV)	M_γ	dM_γ	E_{lab} (MeV)	M_γ	dM_γ
110.0	7.18	0.34	121.5	6.57	0.21	168.9	7.22	0.52
112.0	7.35	0.20	122.5	6.79	0.14	170.9	7.97	0.47
114.0	8.54	0.14	123.5	7.11	0.11	172.0	9.01	0.33
114.8	9.65	0.36	124.7	7.91	0.06	174.0	7.81	0.88
115.5	9.06	0.15	127.4	8.85	0.05	174.9	7.85	0.58
117.8	10.54	0.18	129.9	9.77	0.03	174.9	9.65	0.25
118.2	9.99	0.15	132.9	10.95	0.07	177.4	9.95	0.37
120.1	11.50	0.13	135.0	12.04	0.08	178.8	10.19	0.31
121.2	11.40	0.21	140.0	14.00	0.07	180.8	11.76	0.32
124.0	12.71	0.20	145.0	15.38	0.13	184.3	12.96	0.33
124.0	13.21	0.63	149.1	16.64	0.07	187.6	13.87	0.22
124.1	12.01	0.19	155.2	17.59	0.07	190.0	14.59	0.25
124.1	12.42	0.18	159.8	18.39	0.07	192.6	15.59	0.19
127.4	13.13	0.20	164.9	18.82	0.09	194.9	16.05	0.20
130.6	14.94	0.17				198.5	16.78	0.37
132.4	14.85	0.22				200.0	16.45	0.59
132.9	15.33	0.10				200.0	17.49	0.21
136.2	15.12	0.10				205.8	17.78	0.38
137.5	15.93	0.26				209.4	17.33	0.20
138.2	16.73	0.12				213.3	17.98	0.29
141.3	16.36	0.14				216.0	17.33	0.22
144.8	17.28	0.16				219.9	18.08	0.26
145.3	16.88	0.10				223.1	17.55	0.22

With this setup the average γ multiplicity is given by

$$M_\gamma = \frac{N_{\text{coin}}}{N_{\text{sing}} \times \varepsilon_{\text{NaI}}} \times \varepsilon_n \ , \tag{1}$$

where N_{coin} is the number of ER's in coincidence with a γ ray, N_{sing} is the total number of ER's detected, and ε_{NaI} is the total efficiency for the NaI detectors. The last term, ε_n, is a correction for neutrons interacting with the NaI detectors. This has been determined to be ~ 0.9 in the mass region of our compound nucleus [16].

The identification of the ER's is from a two-dimensional plot of the energy versus the time of flight for each particle. By comparing the singles and coincidence spectra the ER's can be easily distinguished from the projectile-like nuclei. A two-dimensional gate can then be drawn around the ER and projected onto the TOF axis. This process removes the majority of the background under the ER peak. Figure 1(a) demonstrates a typical two-dimensional gate around the ER's in a typical singles spectrum. Figure 2(a) shows the projection of the two-dimensional gate in Fig. 1(a) onto the TOF axis. The gate in Fig. 2(a) indicates the channels used to determine the γ multiplicity. The same gates used in the singles spectra are also used for the corresponding coincidence spectra [Figs. 1(b) and 2(b)].

In Fig. 3, the γ multiplicities are plotted as function of excitation energy in the compound nucleus for each system. The setup of our multiplicity experiment is in-

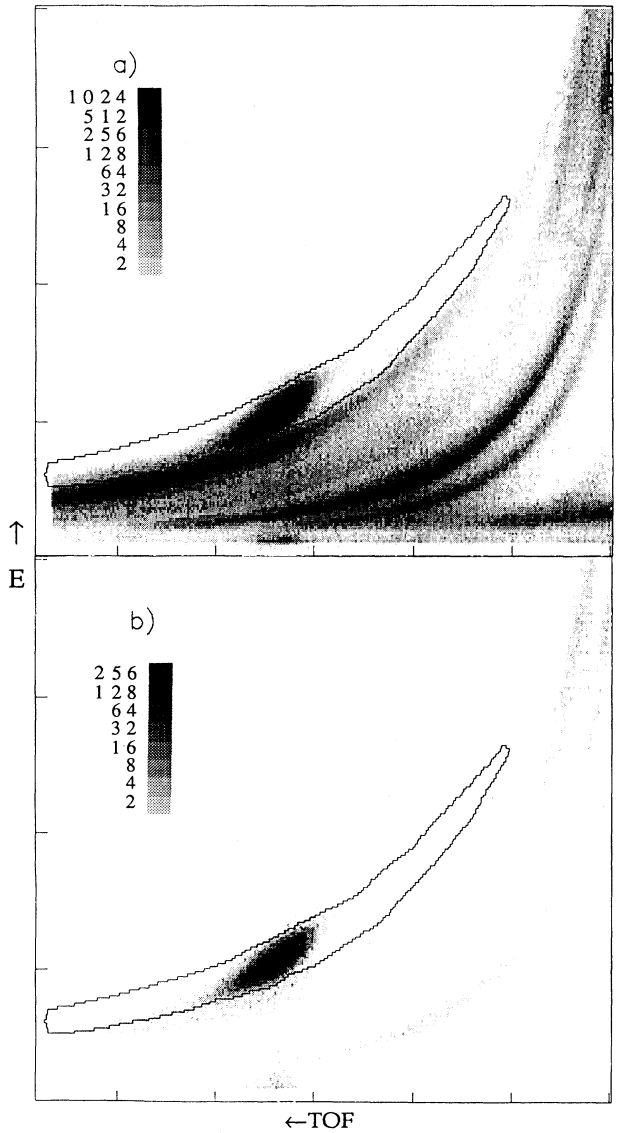

FIG. 1. Energy vs TOF spectrum for ^{32}S + ^{138}Ba at 135.0 MeV in the lab. Singles and coincidence spectra shown in (a) and (b), respectively. The solid curve is a two-dimensional gate around the ER's and extending into the background region. Additional two-dimensional gates (not shown) are used to determine the shape of the background used in Fig. 2. The same gates are used for the coincidence spectrum. The energy and TOF scales are in arbitrary units.

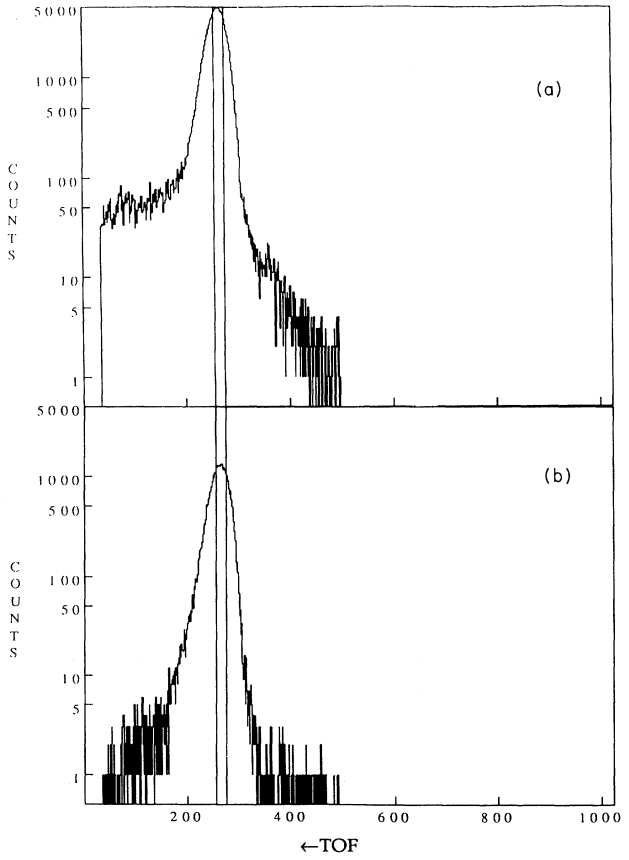

FIG. 2. Gated TOF spectrum for ^{32}S + ^{138}Ba at 135.0 MeV in the lab. The spectrum in (a) is gated by the two-dimensional gate shown in Fig. 1(a) and the spectrum in (b) is gated off the gate shown in Fig. 1(b). The background under the ER peak is shown in both panels. The shape of the background is provided from other two-dimensional gates (not shown) in Fig. 1 placed below and adjacent in the spectrum to the two-dimensional gate shown in Figs. 1(a) and (b). The channels used for determining the peak area are also shown. The same gate is used in both the singles and coincidence spectra. The horizontal axis is labeled in channel number.

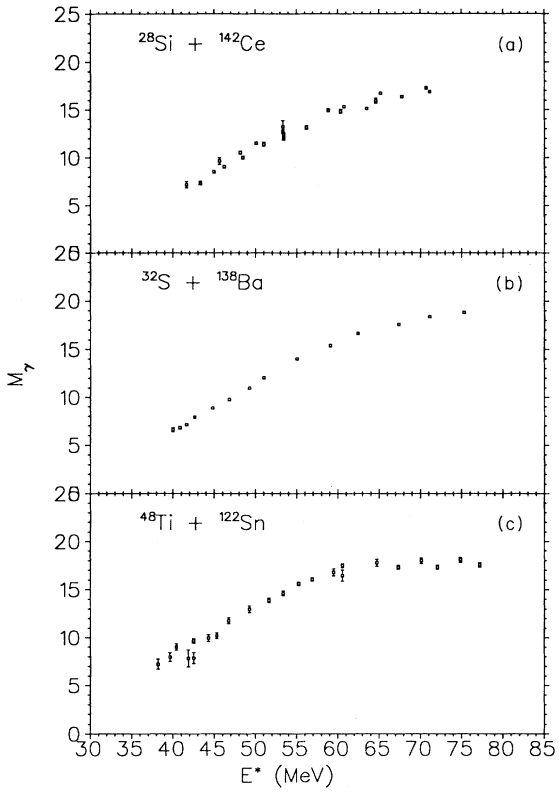

FIG. 3. Experimental γ multiplicities for ^{28}Si + ^{142}Ce, ^{32}S + ^{138}Ba, and ^{48}Ti + ^{122}Sn as a function of excitation energy in the compound nucleus.

sensitive to the fraction of the spin distribution that leads to fission since the fission primarily occurs before γ-ray emission and the fission fragments are not identified in the ER detector. Thus the γ multiplicity is sampling only the portion of the spin distribution that leads to ER formation. This portion of the spin distribution changes little once fission becomes a significant fraction of the fusion cross section. Thus, the γ multiplicity will approach a saturation point as the fission cross section grows. This is evident in Figs. 3(b) and (c) by the saturation of the γ multiplicity at higher excitation energies.

III. CONVERSION OF MULTIPLICITY TO MEAN SPIN

The conversion of multiplicity to mean spin is probably the most controversial of procedures in sub-barrier fusion research. The methods used are subject to model dependencies and many approximations. This is one reason for the problems in comparing the results between the different systems studied to date. To alleviate some of the difficulties in determining the mean spin, the statistical model analysis of the three systems studied here have been done simultaneously using a fixed parameter set. The details of our PACE calculations are discussed in [25,29].

The only input parameter that changed in the PACE calculations at each bombarding energy was the spin distribution of the compound nucleus. The spin distributions were extracted from the coupled-channels fit to the fusion excitation function of the respective fusion system at each energy [25]. The overall agreement with the experimental data is generally acceptable for all three systems. However, in the ^{48}Ti + ^{122}Sn system the PACE calculations are unable to reproduce the $3n$ channel yield [25]. The reason for the discrepancy is a mystery. We were unable to reproduce the $3n$ curve for this system with any reasonable set of parameters, even when trying to fit the ^{48}Ti + ^{122}Sn data alone. The discrepancy in fitting the yield curves for this system is translated into extracted mean spins as a slight lowering of the mean spin at all energies relative to the coupled-channels predictions for the ^{48}Ti + ^{122}Sn system.

For the conversion of multiplicity into mean spin we used a modified version of the procedure proscribed by Halbert *et al.* [17]. This procedure accounts for the various decay properties of each ER channel separately to calculate the average spin for that channel. The mean spin is then the weighted sum over all ER channels (and fission when present). This method is necessarily limited in that the multiplicity for each ER channel is not independently measured. However, for average properties of the spin distribution the method is sufficient. The mean compound nuclear angular momentum is given by

$$\langle l \rangle = \left[\sum_i^{\text{chnl}} f_i \times [2(M_\gamma - M_{si} + B_{bi}) + k_i] \right] + f_{\text{fiss}} \cdot J_{\text{fiss}} \ , \tag{2}$$

where M_γ is the measured γ multiplicity and k_i is given by

$$k_i = M_{si} \cdot J_{si} + M_{ni} \cdot J_{ni} + M_{pi} \cdot J_{pi} + M_{\alpha i} \cdot J_{\alpha i} \ . \tag{3}$$

In Eqs. (2) and (3), M_{xi} and J_{xi} are the average multiplicity of and average spin removed by x, respectively, where $x = n$, p, α, represents neutron, proton, or alpha-particle evaporation, respectively, and $x = s$ represents statistical γ-ray emission for channel i with yield f_i. The fraction of the spin distribution that leads to fission is given by f_{fiss} and the average spin of this fraction is given by J_{fiss}.

The qualitative interpretation of the

$$\sum_i^{\text{chnl}} f_i \times [2(M_\gamma - M_{si} + B_{bi}) + k_i]$$

term is that the $M_\gamma - M_{si}$ observed γ's plus the B_{bi} unobserved γ's are stretched quadrupole transitions carrying away two units of angular momentum. This interpretation is only valid when used in summation over the exit channel since M_γ is not determined for individual channels. The M_{si} "statistical" γ rays are mostly dipole γ rays early in the cascade which do not carry away any angular momentum on the average. This latter extreme assumption is corrected for in the k_i term which takes into account the statistical model estimate of the angu-

lar momentum removed by particles and statistical γ's.

The J's and M's in Eqs. (2) and (3) are extracted from the PACE calculations at each energy. A correction term (B_{bi}) is included for each channel to correct for the missing multiplicity from internal conversion and the absorption of low-energy photons. This correction term was first introduced in [24] where this recipe for connecting multiplicity to spin was calibrated by studying a similar composite system formed by a light ion at above barrier energies. In this latter situation the spin distribution can be reliably estimated from *a priori* information. The size of the correction term varies for each ER from a value of about 0.5 for even-even nuclei to about 3.0 for odd-odd nuclei. The overall error in the mean spin expected from the uncertainty in the B_{bi} term is estimated to be approximately $1\hbar$ or less. Figure 4 shows the results of the conversion process for each system.

IV. COMPARISON WITH COUPLED-CHANNELS MODEL

In this section we will compare the mean spins determined from the γ-ray multiplicities with the result of a coupled-channels model. This model is appealing because it has a minimum of adjustable parameters none of which will be fit to improve the comparison with the mean-spin data. The dominant couplings are due to the known low-lying quadrupole and octupole states of the target and projectile nuclei. The only adjustable parameter in our approach is the strength of the nuclear potential which determines the height of the $l = 0$ barrier in the absence of couplings. This strength is fine-tuned from a global parametrization to reproduce the fusion excitation function. The code CCDEF [30] was used to perform the calculations.

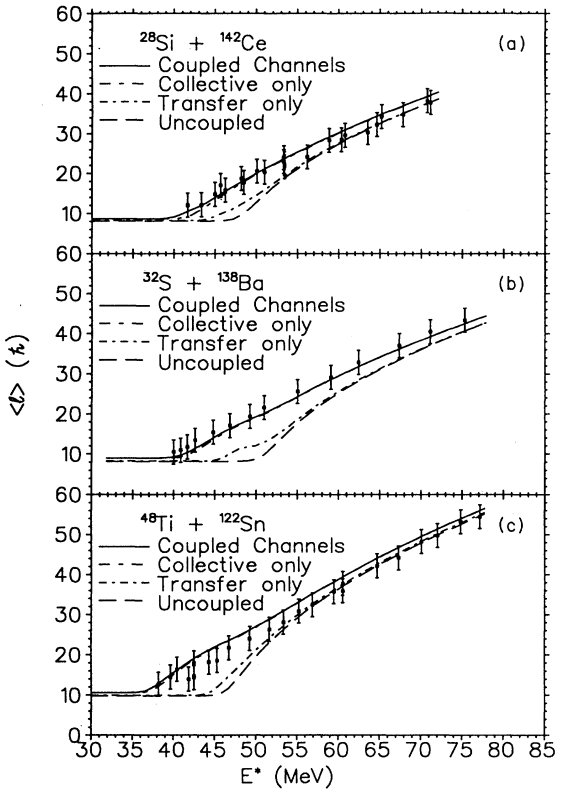

FIG. 4. Mean spins for ^{28}Si + ^{142}Ce, ^{32}S + ^{138}Ba, and ^{48}Ti + ^{122}Sn as a function of excitation energy in the compound nucleus. The solid curves are the predictions of our CCDEF calculation that fits the fusion excitation function for each system, respectively. The dashed curves are the CCDEF predictions with some or all of the couplings removed as described in [25]. The collective only and collective+transfer curves are generally indistinguishable.

The fitting of the fusion cross sections with the CCDEF code is discussed in [26] and described in detail in [31]. This analysis included the lowest-lying quadrupole and octupole states of both the target and the projectile for all of the systems. The quadrupole state ($|\beta_2| \geq 0.27$) for each of the projectiles was coupled in as a static deformation of the nucleus. The quadrupole state ($|\beta_2| \leq 0.12$) for each of the targets and the first octupole state for all nuclei were coupled in as surface vibrational states. The deformation parameters (β_2 and β_3) for all nuclei were taken from literature values [32,33]. A one-neutron transfer channel was also included in the calculations. The Q value for a one-neutron pickup reaction was used for each system. It is shown elsewhere [26] that inclusion of other transfer channels has a very small effect.

The fusion cross sections can be fit [26] quite well for all three systems by a fine-tuning of the barrier position by adjustment of the strength of the nuclear potential. We show here, Fig. 4, the results of these calculations for the dependence of the mean spin as a function of excitation energy for the three systems. There has been no additional parameter adjustment. The model generally reproduces the mean spin throughout the barrier region for all three cases. The model does tend to overpredict the experimental ^{48}Ti + ^{122}Sn results by a small amount (1–2 $\hbar$) not clearly outside our experimental uncertainties. This may be related to the inability to fit the partial yields for this system with statistical model calculations [25].

The enhancement of the mean spin over the results of calculations with no coupling is well reproduced by the coupled-channels model for all three systems. This along with the fits to the fusion excitation functions would indicate that there are no entrance channel effects in these systems that are not accounted for in the coupled-channels formalism using known collectivities of the projectile and target nuclei. We also show in Fig. 4 that this enhancement arises primarily from collective excitations rather than transfer.

V. CONCLUSIONS

The fusion cross sections and mean spins have been measured for three systems that produce the same compound nucleus in the energy range fom 10% below to 20% above the BPM fusion barrier. The systems studied were ^{28}Si + ^{142}Ce, ^{32}S + ^{138}Ba, and ^{48}Ti + ^{122}Sn which all produce the compound nucleus ^{170}Hf. The fusion excita-

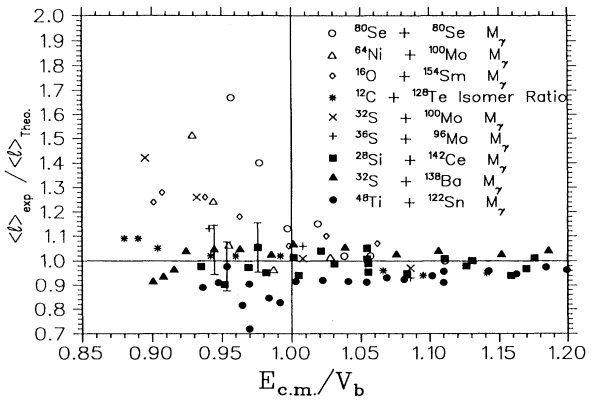

FIG. 5. Systematics of the $\langle l \rangle$ for the present study. The ratio of the experimental $\langle l \rangle$ to the $\langle l \rangle$ from the coupled-channels fits to the fusion excitation function as a function of center-of-mass energy relative to the fusion barrier. The results of the present study are presented as the solid data points (square, triangle, and circle for ^{28}Si $+^{142}$Ce, ^{32}S $+^{138}$Ba, and ^{48}Ti $+^{122}$Sn, respectively). Also shown are the systematics for several systems measured previously. The data for the other systems come from [3].

tion functions and mean spin distributions for all three systems were well reproduced by coupled-channels calculations with the code CCDEF over the entire energy range. Comparison between the systems shows no strong evidence for a mass asymmetry effect on the fusion process. In Fig. 5 the ratio of the experimental mean spins to the model calculated mean spins as a function of center-of-mass energy relative to the fusion barrier is plotted for all three systems. The systems in this study show none of the discrepancies between experiment and theory that have been seen in other systems such as the ^{32}S $+^{100}$Mo and ^{64}Ni $+^{100}$Mo systems. In the latter two systems the mean spin substantially exceeds expectations at sub-barrier energies.

The problem with reproducing the mean spins is a real one for several systems [3]. However, this study does indicate that the answer to the problem is not directly related to the mass asymmetry of the entrance channel. More likely, the problem is probably related to nuclear structure effects that have not been included in the models or possibly to multiparticle transfer processes. The transfer of multiple particles between nuclei is not completely understood and the fusion models usually treat it as sequential single-particle transfers. There is also the possibility that the deduction of the mean spin from the experimental observable is not completely correct in some cases. These possibilities need to be further explored both theoretically and experimentally.

One possible extension of our study would be the symmetric system ^{82}Se $+^{88}$Sr. This system also leads to the compound nucleus ^{170}Hf in the same excitation energy range as the systems studied here. Measurement of the fusion excitation function and mean spins for this system would extend this study into the region of mass asymmetry where the largest discrepancy between the fusion models and the experimental results are currently found. This system was not included in the present study due to accelerator limitations at the Nuclear Physics Lab [31].

This work was supported in part by the U.S. Department of Energy and the National Science Foundation.

[1] M. Beckerman, Phys. Rep. **129**, 145 (1985).
[2] S. Steadman and M. Rhoades-Brown, Annu. Rev. Nucl. Sci. **36**, 649 (1986).
[3] R. Vandenbosch, Annu. Rev. Nucl. Sci. **42**, 447 (1992).
[4] H. Esbensen and S. Landowne, Phys. Rev. C **35**, 2090 (1987).
[5] H. Esbensen and S. Landowne, Nucl. Phys. A **492**, 473 (1989).
[6] P. H. Stelson, Phys. Lett. B **205**, 190 (1988).
[7] P. H. Stelson, H. J. Kim, M. Beckerman, D. Shapira, and R. L. Robinson, Phys. Rev. C **41**, 1584 (1990).
[8] C. E. Aguiar, L. F. Canto, and R. Donangelo, Phys. Rev. C **31**, 1969 (1985).
[9] C. E. Aguiar, V. C. Barbosa, L. F. Canto, and R. Donangelo, Phys. Rev. C **38**, 541 (1988).
[10] B. T. Kim, T. Udagawa, and T. Tamura, Phys. Rev. C **33**, 370 (1986).
[11] T. Udagawa, B. T. Kim, and M. Naito, Phys. Rev. C **45**, 876 (1992).
[12] A. B. Balantekin, J. R. Bennett, and S. Kuyucak, Phys. Rev. C. **48**, 1269 (1993).
[13] N. Rowley, J. R. Leigh, J. X. Wei, and R. Lindsay, Phys. Lett. B **254**, 25 (1991).
[14] J. X. Wei, J. R. Leigh, D. J. Hinde, J. O. Newton, R. C. Lemmon, S. Elfstrom, J. X. Chen, and N. Rowley, Phys. Rev. Lett. **67**, 3368 (1991).
[15] N. Rowley, G. R. Satchler, and P. H. Stelson, Phys. Lett. B **314**, 179 (1993).
[16] S. Gil, Ph.D. thesis, University of Washington, 1985.
[17] M. L. Halbert, J. R. Beene, D. C. Hensley, K. Honkanen, T. M. Semkow, V. Abenante, D. G. Sarantites, and Z. Li, Phys. Rev. C **40**, 2558 (1989).
[18] P. Fröbich and J. Richert, Phys. Lett. B **237**, 328 (1990).
[19] R. G. Stokstad, D. E. DiGregorio, K. T. Lesko, B. A. Harmon, E. B. Norman, J. Pouliot, and Y. D. Chan, Phys. Rev. Lett. **62**, 399 (1989).
[20] J. D. Bierman, A. W. Charlop, D. J. Prindle, R. Vandenbosch, and D. Ye, Phys. Rev. C **48**, 319 (1993).
[21] T. Murakami *et al.*, Phys. Rev. C **34**, 1353 (1986).
[22] H.-J. Hennrich, G. Breitbach, W. Kühn, V. Metag, R. Novotny, D. Habs, and D. Schwalm, Phys. Lett. B **258**, 275 (1991).
[23] P. J. Nolan, D. J. G. Love, A. Kirwan, D. J. Unwin, A. H. Nelson, P. J. Twin, and J. D. Garrett, Phys. Rev. Lett. **54**, 2211 (1985).
[24] S. Gil, R. Vandenbosch, A. Charlop, A. Garcia, D. D. Leach, S. J. Luke, and S. Kailas, Phys. Rev. C **43**, 701 (1991).
[25] S. Gil *et al.*, unpublished.
[26] A. Charlop, J. Bierman, Z. Drebi, A. Garcia, S. Gil, D. Prindle, A. Sonzogni, R. Vandenbosch, and D. Ye, the preceding article, Phys. Rev. C **51**, 623 (1994).

[27] A. Charlop *et al.*, Phys. Rev. C **49**, R1235 (1994).
[28] Micromatter, P. O. Box 123, Deer Harbor, Washington 98243-0123, USA.
[29] A. Gavron *et al.*, Phys. Rev. Lett. **52**, 589 (1984).
[30] J. Fernandez-Niello, C. Dasso, and S. Landowne, Comput. Phys. Commun. **54**, 409 (1989).
[31] A. W. Charlop, Ph.D. dissertation, University of Washington, 1993.
[32] S. Raman, C. Malarkey, W. Milner, C. Nestor, Jr., and P. Stelson, Nucl. Data Tables **36**, 1 (1987).
[33] R. Spear, Nucl. Data Tables **42**, 55 (1989).

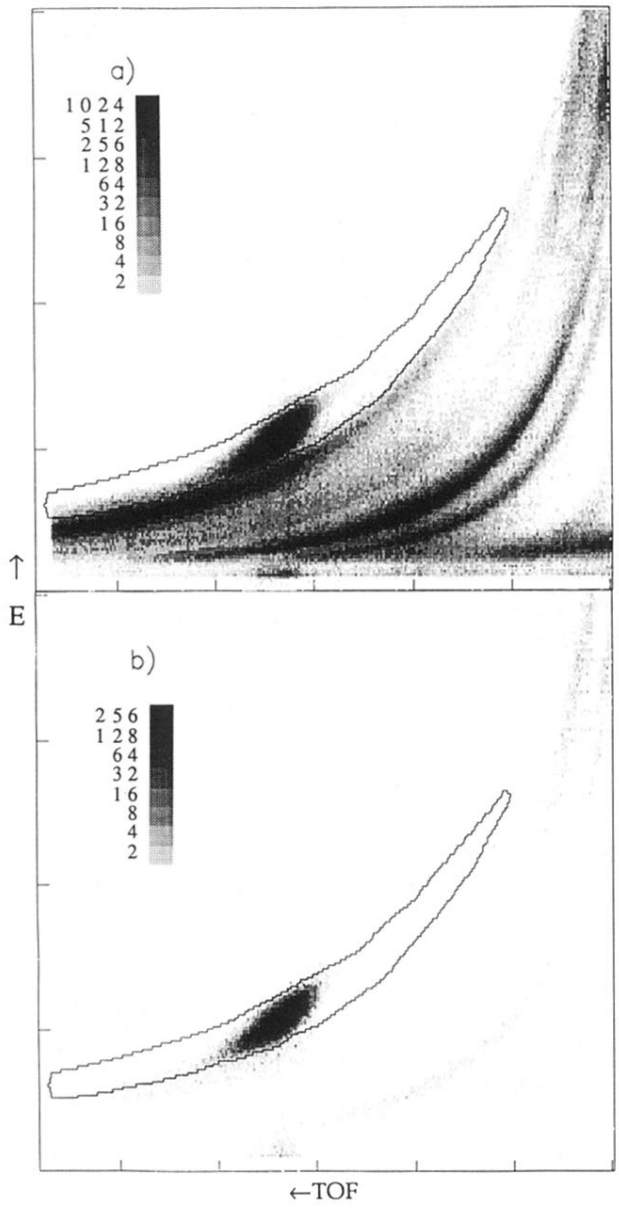

FIG. 1. Energy vs TOF spectrum for $^{32}S + ^{138}Ba$ at 135.0 MeV in the lab. Singles and coincidence spectra shown in (a) and (b), respectively. The solid curve is a two-dimensional gate around the ER's and extending into the background region. Additional two-dimensional gates (not shown) are used to determine the shape of the background used in Fig. 2. The same gates are used for the coincidence spectrum. The energy and TOF scales are in arbitrary units.